

Phase diagram for condensation of microcavity polaritons: from theory to practice

F. M. Marchetti,¹ M. H. Szymańska,² J. M. J. Keeling,³ J. Kasprzak,^{4,*} R. André,⁴ P. B. Littlewood,³ and Le Si Dang⁴

¹*Rudolf Peierls Centre for Theoretical Physics, 1 Keble Road, Oxford OX1 3NP, UK*

²*Department of Physics, University of Warwick, Coventry CV4 7AL, UK*

³*Cavendish Laboratory, University of Cambridge, Madingley Road, Cambridge CB3 0HE, UK*

⁴*CEA-CNRS-UJF joint group 'Nanophysique et Semiconducteurs',
Institut Néel, CNRS, 25 rue des Martyrs, 38042 Grenoble, France*

(Dated: March 23, 2007)

The first realization of a polariton condensate was recently achieved in a CdTe microcavity [Kasprzak *et al.*, Nature **443**, 409 (2006)]. We compare the experimental phase boundaries, for various detunings and cryostat temperatures, with those found theoretically from a model which accounts for features of microcavity polaritons such as reduced dimensionality, internal composite structure, disorder in the quantum wells, polariton-polariton interactions, and finite lifetime.

PACS numbers: 71.35.Lk, 03.75.Gg, 71.36.+c

I. INTRODUCTION

Microcavity polaritons^{1,2} are the quasi-particles which result from strong light-matter coupling in semiconductor microcavities. The light polariton mass means a weakly interacting dilute Bose gas picture would imply a high transition temperature^{3,4,5} and, even with more sophisticated methods,^{6,7,8} the expected transition temperature is 10^8 times higher than for atomic gases. While Bose-Einstein condensates (BEC) of atomic gases are now routinely studied, condensation of microcavity polaritons has been long sought^{9,10,11,12,13,14,15} and only recently has a thermal equilibrium condensate accompanied by spontaneous coherence been realized in a CdTe microcavity.¹⁶ In the same structure the polarisation has been investigated,¹⁷ second order temporal coherence has been studied,¹⁸ and pinned vortices have been observed in the condensed phase.¹⁹ Spontaneous coherence of microcavity polaritons has been also recently investigated in GaAs,^{20,21} while there have been early reports on room temperature polariton lasing in a GaN cavity.²²

Microcavity polaritons are interacting particles in a disordered potential with internal structure and finite lifetime, which form a finite two-dimensional gas, so their condensation differs from that of ideal non-interacting three-dimensional (3D) bosons for which BEC was originally discussed. It is therefore crucial to establish these differences and the nature of polariton condensation. To this end, the aim of this paper is to compare theoretical and experimental results for the phase diagram, and to discuss what they reveal about the nature of the polariton condensate. We discuss both complete thermal equilibrium phase diagrams, and also consider effects that may result from pumping and decay (even when the polariton distribution is well thermalised). As a further way of illustrating the differences between the ideal 3D Bose gas and microcavity polaritons, the condensate fraction as a function of pumping strength is presented; this is compared qualitatively to a theoretical model including effects of pumping and decay.

We experimentally evaluate the critical density for

condensation at low cryostat temperatures in the range $T_{\text{cryo}} = (5, 15)\text{K}$ and for exciton-photon detunings in the range $\delta = (5.3, 12.5)\text{meV}$. These densities are compared with the predictions of a realistic microscopic model that accounts for the composite structure of microcavity polaritons, interactions enhanced by quantum well disorder and finite polariton lifetime. This comparison reveals two crucial aspects of the current realisation of polariton condensation in CdTe: that it lies in the crossover between BEC of weakly interacting bosons and the mean-field phase transition driven by interactions; and that the excitonic disorder is important in the evaluation of the polariton-polariton interactions.

The organisation of the remainder of this paper is as follows: Section II describes the experimental estimate of critical density, found by integrating the occupation. Section III then introduces the theoretical models we consider, and in Sec. IIIC we discuss the various theoretical estimates of phase boundaries they produce. The comparison between the various estimates of experimental critical density and the theoretical phase boundary is shown in Sec. IV. The effects of pumping and decay are discussed in Sec. V, and their influence on the condensate fraction – in Sec. V A.

II. EXPERIMENTAL DETERMINATION OF CRITICAL DENSITY

A CdTe/CdMgTe microcavity with 16 quantum wells and Rabi splitting $\Omega_R = 26\text{meV}$, is non-resonantly pumped at the first high energy lobe of the Bragg structure, at 1.768eV (about $\sim 100\text{meV}$ above the lower polariton ground state energy) by a continuous-wave Ti:sapphire laser combined with an acousto-optic modulator ($1\mu\text{s}$ pulse duration with a duty cycle of 1%) to reduce the sample heating. The excitation spot is uniform and of $\sim 35\mu\text{m}$ diameter. Following Ref.16, we detune the photon energy ω_k above the exciton E_x ($\delta = \omega_0 - E_x$) and, increasing the pump laser power, we measure the energy- and angle- (or momentum-) resolved emission in-

tensities via far-field spectroscopy (inset of Fig. 1). In-plane momentum \mathbf{k} and emission angle $\theta_{\mathbf{k}}$ are related by $\hbar c|\mathbf{k}| = E_{\mathbf{k}}^{\text{LP}} \sin \theta_{\mathbf{k}}$, where

$$E_{\mathbf{k}}^{\text{LP,UP}} = \frac{1}{2}[\omega_{\mathbf{k}} + E_x \mp \sqrt{(\omega_{\mathbf{k}} - E_x)^2 + \Omega_R^2}]$$

are the lower (LP) and upper polariton (UP) energies. From the energy-integrated photoluminescence (PL) at a given momentum $\mathcal{P}_{\mathbf{k}}$, the occupation $\mathcal{O}_{\mathbf{k}}$ of that state is given by²³

$$\mathcal{O}_{\mathbf{k}} = \frac{\mathcal{P}_{\mathbf{k}}}{\cos^4 \theta_{\mathbf{k}} c_{\mathbf{k}}^2}, \quad c_{\mathbf{k}}^2 = \frac{1}{2} \left[1 - \frac{\omega_{\mathbf{k}} - E_x}{\sqrt{(\omega_{\mathbf{k}} - E_x)^2 + \Omega_R^2}} \right].$$

By finding the energy at which, for a given momentum, the PL is maximum, momentum dependence can be converted to energy dependence; an example is shown in Fig. 1. Above a threshold pump power, the ground state occupation grows exponentially, while the effective LP temperature, T_{eff} , (extracted from the tail of the occupation) does not change much. This macroscopic occupation of the ground state has been shown to be associated with macroscopic coherence across the spot size,¹⁶ demonstrating polariton condensation. At threshold $T_{\text{eff}} = 16\text{K}$; this is above T_{cryo} because the polariton lifetime (of 1–2ps) is shorter than typical relaxation times (although longer than their thermalization time).^{15,16} The ground state occupation at threshold is, within a factor of two, measured to be one; in Fig. 1 this is rescaled to one.

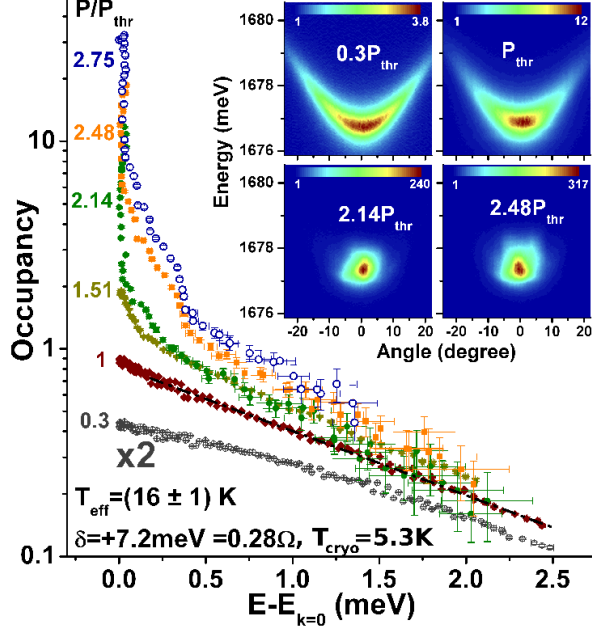


FIG. 1: (Color online) LP occupation versus energy at various excitation powers extracted from the energy-resolved far-field emission (inset).

The LP density at the threshold pump power can then be estimated by integrating the occupation to give the

total density. The estimate found this way is represented on Fig. 3 by blue stars. Since the system is thermalized, by rescaling the occupation at $\mathbf{k} = 0$ to one, this density estimate is determined by the effective temperature only; any variation at fixed temperature is due to changes to the LP density of states.

III. THEORETICAL PHASE DIAGRAMS

This section discusses the theoretical modelling of the phase diagram, and further methods of estimating the experimentally observed critical density. The discussion here concerns the thermal equilibrium case; possible effects of pumping and decay are discussed later in Sec. V. The discussion will compare the use of two models; the first — model (1) — is a model of disorder localised saturable excitons coupled to propagating photons.^{7,24} At low enough densities and temperatures, the critical density given by model (1) will be dominated by long wavelength bosonic fluctuations,^{6,25} and so the results of this model can be reproduced by modelling lower polaritons as a weakly interacting dilute Bose gas,^{5,23,26} which we shall call model (2). Excitonic disorder can significantly modify the effective polariton interaction compared to the clean case. To take account of excitonic disorder in model (2), we choose the interaction strength for this model so as to match the low density limit of model (1), in which excitonic disorder is explicitly considered. Such matching is achieved by calculating the form of blueshift vs density in both models, and choosing the effective interaction strength for the bosonic model so they agree. This calculation of blueshift vs density also allows a second estimate of the experimentally found critical density, by measuring the blueshift observed at that density.

A. Localised exciton model

The first model, following Refs.7,24, starts from the single-particle exciton states (numerically) evaluated in a disordered quantum well, as explained further below. Although being 2D, all such states are localised, the nature of the exciton states and their associated oscillator strength change substantially with the exciton energy.²⁷ The exciton states that couple most strongly to the cavity photons are those just below the band edge.

Although the exciton states are localised, polaritons consist of a superposition of many excitons²⁸ and so need not be localised.²⁹ Polaritons in CdTe are also localised by photonic disorder, associated with the spatial inhomogeneity observed in the PL above threshold. However, above threshold, coherence can be observed over a large length scale approaching the excitation spot size,^{16,30} and so polaritons could not be localised on a shorter length scale. This gives an energy scale up to $0.1\text{meV} \simeq 1\text{K}$, much smaller than the observed blue-shift (due to interaction). This difference in energy scales suggests that

localisation is a perturbation to a theory of interacting bosons, rather than vice versa; we therefore neglect photonic disorder when finding the phase boundary.

1. Many body Hamiltonian

In the many body Hamiltonian, we approximate the interactions between excitons by exclusion: Each single-particle exciton state can only be occupied once. This approximation over-estimates the on-site interaction and neglects the inter-site interaction — in reality there is finite Coulomb and exchange energy to multiply occupy the same single exciton states. However, as discussed in Ref.26, this approximation is valid at low enough densities. This procedure yields model (1),

$$\hat{H} = \sum_{\alpha} \varepsilon_{\alpha} S_{\alpha}^z + \sum_{\mathbf{k}} \omega_{\mathbf{k}} \psi_{\mathbf{k}}^{\dagger} \psi_{\mathbf{k}} + \frac{1}{\sqrt{A}} \sum_{\alpha, \mathbf{k}} (g_{\alpha, \mathbf{k}} \psi_{\mathbf{k}} S_{\alpha}^{+} + \text{h.c.}) \quad (1)$$

The spin operators S^z, S^{\pm} describe states $|\uparrow_{\alpha}\rangle$ and $|\downarrow_{\alpha}\rangle$ corresponding respectively to the presence or absence of an exciton of energy ε_{α} . The operators $\psi_{\mathbf{k}}$ describe confined photon modes of energy $\omega_{\mathbf{k}} = \omega_0 + \hbar^2 \mathbf{k}^2 / 2m_{\text{ph}}$ and $m_{\text{ph}}/m_0 = 2.58 \times 10^{-5}$ (m_0 is the bare electron mass). The quantisation area A that appears in Eq. (1) plays no role in any final answer, and is taken to infinity in all our calculations. The Hamiltonian written in Eq. (1) does not yet take account of spin of the exciton states or polarisation states of the light. To a first approximation, the interaction between different spins is weak; in such a limit each polarisation behaves separately, and one has independent copies of this model for each spin, thus introducing a degeneracy factor $g_s = 2$ in the total density. Beyond this limit, opposite spin polarisations are weakly attractive, producing bound excitonic states; the effect of such an interaction is discussed in Appendix A.

2. Energies and coupling strength of excitons

As in Refs.7,24, the exciton energies ε_{α} and coupling strengths $g_{\alpha, \mathbf{k}}$ (which lead to the inhomogeneous exciton linewidth) are taken from numerical diagonalisation of exciton wavefunctions in a disorder potential.²⁷ These numerical calculations are described in detail in Ref.24, so we only briefly summarise the method here. We numerically solve the Schrodinger equation in a disorder potential:

$$\left[-\frac{\nabla_{\mathbf{R}}^2}{2m_x} + V(\mathbf{R}) + E_x \right] \Phi_{\alpha}(\mathbf{R}) = \varepsilon_{\alpha} \Phi_{\alpha}(\mathbf{R}).$$

We use the CdTe exciton mass³¹ $m_x/m_0 = 0.6$, and a Gaussian correlated exciton disorder. For disorder weaker than the exciton binding energy, the internal

structure of the exciton smooths disorder on lengthscales shorter than the exciton Bohr radius²⁷ a_x , so we can consider a Gaussian noise correlated on a length scale ℓ_c :

$$\langle V(\mathbf{R}) \rangle = 0, \quad \langle V(\mathbf{R}) V(\mathbf{R}') \rangle = \frac{\sigma^2 \ell_c^2}{A} \sum_{\mathbf{q}} e^{i\mathbf{q} \cdot (\mathbf{R} - \mathbf{R}')} \quad 1/\ell_c.$$

We take $\ell_c = 167 \text{\AA} \gtrsim a_x$ and so the only free parameter in this calculation is the strength σ of the disorder; this was chosen to give an exciton linewidth that matches the observed CdTe exciton linewidth ($\sim 1 \text{meV}$), leading to $\sigma = 0.79 \text{meV}$.

The exciton-photon coupling strength involves the overlap between the disorder localised exciton state, and the photon wavefunction. Since the relevant photon momenta are small compared to the typical scales of the exciton wavefunction (i.e. small compared to $1/a_x$), we take this coupling strength at zero photon momentum, as $g_{\alpha, \mathbf{k}} \simeq g_{\alpha, 0} \propto \langle \Phi_{\alpha} | \mathbf{k} = 0 \rangle$, where Φ_{α} is the disorder localised exciton state. To fix the overall scale of the couplings we use Rabi splitting $\Omega_R = 2\sqrt{\sum_{\alpha} |g_{\alpha, 0}|^2 / A}$ with the observed Rabi splitting. Thus, the complete set parameters defining model (1) are the exciton mass, the Rabi splitting, the exciton linewidth, the exciton Bohr radius and the photon mass. These parameters all have reasonably well established values, and are not used as fitting parameters.

B. Weakly interacting dilute Bose gas

At low densities and temperatures, the thermodynamics of model (1) is dominated by long wavelength bosonic fluctuations,^{6,25} and so it gives the same predictions as an effective LP model^{5,23,26} [model (2)]:

$$\hat{H} \simeq \sum_{\mathbf{k}} E_{\mathbf{k}}^{\text{LP}} L_{\mathbf{k}}^{\dagger} L_{\mathbf{k}} + \sum_{\mathbf{k}, \mathbf{k}', \mathbf{q}} V_{\mathbf{k}, \mathbf{k}', \mathbf{q}}^{\text{eff}} L_{\mathbf{k}+\mathbf{q}}^{\dagger} L_{\mathbf{k}'-\mathbf{q}}^{\dagger} L_{\mathbf{k}'} L_{\mathbf{k}} \quad (2)$$

As before, in the absence of biexcitonic effects, the spin degree of freedom only contributes a factor $g_s = 2$ to the density. Such a model for the condensation of weakly interacting bosons is often studied in the context of excitons, and of atomic gases.³² For polaritons, model (2) has been considered^{3,4} with the interaction strength $V_{\mathbf{k}, \mathbf{k}', \mathbf{q}}^{\text{eff}}$ taken from a combination of Coulomb interaction and the nonlinearity of exciton-photon coupling.²³ However, excitonic disorder can significantly enhance polariton-polariton interactions^{7,24} and make them larger than those in clean QWs. In choosing the value of $V_{\mathbf{k}, \mathbf{k}', \mathbf{q}}^{\text{eff}}$ we wish to include these effects of disorder, which are described microscopically in model (1). As mentioned above, the form of model (2) describes the relevant excitations of model (1) at low densities and temperatures, and so the physical predictions of these two models should match in this limit. Hence, the effect of disorder on the interaction strength can be included by choosing the value of $V_{\mathbf{k}, \mathbf{k}', \mathbf{q}}^{\text{eff}}$ so as to make the results

of model (1) and model (2) match at low densities and temperatures.

1. Fixing effective interaction strength

Following the relation between the two models as described above, the value of V^{eff} is chosen so that the blueshift vs density in the normal state calculated in both models will match. In the normal state of model (2), the LP blue-shift varies linearly with the density $\delta E^{\text{LP}} \sim V^{\text{eff}} n$. In model (1) the blue-shift depends on both temperature and disorder, but, in the low density normal state, it also varies approximately linearly (lower panel of Fig. 2). We choose V^{eff} so these gradients are the same. In both models, once condensed, the LP branch locks to the chemical potential, and so the blue-shift traces the dependence of chemical potential on density, increasing more rapidly than linearly at first, before eventually saturating (illustrated by the red \times symbols in the lower panel of Fig. 2).

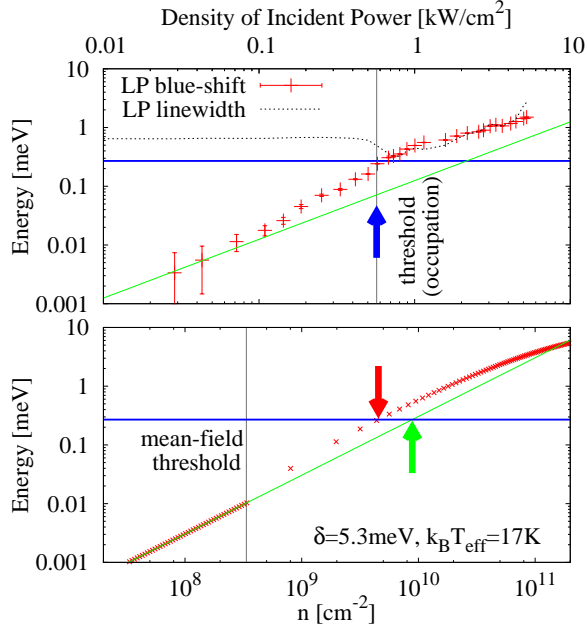


FIG. 2: (Color online) Comparison of (panel a) experimental LP blue-shift (red data with error bars) vs. incident pump power; (bottom panel) theoretical LP blue-shift (red \times symbols) vs. mean-field density. The experimental LP linewidth (black dashed) and threshold (found from the occupation data) are also shown. Measured blue-shifts at threshold can be translated to densities as explained in the text.

The value found by this procedure is $V^{\text{eff}} = 1.52 \mu\text{eV}\mu\text{m}^2$, implying a blue-shift of 0.304 meV at a density of 10^{10} cm^{-2} . This effective interaction strength V^{eff} is roughly 10 times that found from Coulomb and saturation effects in a clean system.²³ The relative size of inter-site Coulomb and saturation effects can also be seen

in the UP energy shift with pump power: The Coulomb term shifts both LP and UP in the same direction, saturation effects lead to opposite shifts. Experimental data in the on-line supplementary information of Ref.16 show an UP red-shift of magnitude comparable to the LP blue-shift, strongly suggesting that saturation effects dominate Coulomb interactions.

2. Estimating experimental density from blueshift

The calculation of blue shift as a function of density allows one to extract a second estimate of the LP density at threshold, by converting the experimentally observed blueshift (Fig. 2, upper panel) to the corresponding density. However, as seen in Fig. 2, the mean-field estimate of blue-shift differs according to whether one considers the condensed or uncondensed case. Since fluctuations beyond the mean-field approximation delay the transition, the actual blue-shift at threshold should lie between the condensed and uncondensed mean-field estimates. Thus, for a given observed blue shift, one can extract two estimates of the density that should bound the actual density. These two translations to density are shown in Fig. 3, as red upward triangles for the condensed calculation, and green downward triangles for the uncondensed case.

C. Theoretical phase boundaries

The experimental estimate of the critical polariton density can be now compared to the theoretical phase diagram. From model (1), one may derive a mean-field phase diagram, for condensation of polaritons in the lowest energy state. The mean-field phase boundary^{24,28} comes from finding the mean-field estimate of density ($g_s = 2$ takes into account the degeneracy introduced by the excitonic spin):

$$n = \frac{1}{A} \sum_{\alpha} \frac{g_s}{2} \left[1 - \tanh \left(\frac{\beta(\varepsilon_{\alpha} - \mu)}{2} \right) \right], \quad (3)$$

at the chemical potential μ which first satisfies the saddle-point equation (which plays a role analogous to the self consistency condition or Gross-Pitaevskii equation for a weakly interacting dilute Bose gas):

$$\omega_0 - \mu = \frac{1}{A} \sum_{\alpha} |g_{\alpha,0}|^2 \frac{\tanh[\beta(\varepsilon - \mu)/2]}{\varepsilon - \mu}. \quad (4)$$

This mean-field boundary is shown as a black solid line in Fig. 3.

Including fluctuation corrections to this mean-field transition, one recovers a smooth crossover from the mean-field limit at higher densities to a fluctuation dominated regime at low densities^{6,25}; in this fluctuation dominated regime, the results of model (1) are equivalent to

those of model (2). This crossover is at a temperature that is controlled by Rabi splitting, and is of the order of one tenth of the Rabi splitting. In 2D, for interacting bosons with a quadratic dispersion, the transition temperature to the superfluid state, the Berezinskii-Kosterlitz-Thouless (BKT)^{33,34} temperature, varies linearly with the density n and is close to the quantum degeneracy temperature, $T_{\text{deg}} \propto n/m$. The results of model (2) are not quite so simple as the dispersion is non-quadratic.^{3,4,5} However, at ultra-low densities, the phase boundary of model (2) (blue dotted-dashed line) recovers a linear dependence of critical temperature on density (black dashed line).

The BKT transition discussed above describes an infinite two-dimensional system. The experimental system however contains photonic disorder, which might act as a trapping potential for polaritons. In a non-interacting harmonically trapped two-dimensional Bose gas, a transition exactly like that described by Bose and Einstein can exist due to the modification of density of states by the harmonic trap.^{35,36} However, the polariton system is interacting, and it is not a-priori valid to ignore interactions; the inclusion of interactions in an harmonically trapped system³⁷ can replace the BEC transition of the non-interacting gas with a transition better described by BKT physics. The exact details of the critical behaviour in a trapped two-dimensional interacting system are delicate. As already discussed in Sec. III A, for the parameters relevant in the current system, the effects of polariton trapping induced by the photonic disorder are weak compared to the polariton-polariton interaction strength. However our interest here is in the prediction of the phase boundary, we note that for the parameters relevant here simple estimates of the critical temperature for the BEC of non-interacting trapped system do not differ significantly from those for the BKT transition. There is a quite separate question concerning coherence (and condensate fraction) in a two dimensional trapped system, which we discuss below in Sec. V A.

IV. COMPARISON OF THEORETICAL AND EXPERIMENTAL BOUNDARIES

In Fig. 3 the experimental density is near the crossover between the low- and high-density parts of the theoretical phase boundary. The density estimated from the blue shift is slightly greater than that from integrating the occupation; however without the effects of excitonic disorder, the density from the blueshift would be ten times higher. Let us consider the possible systematic errors involved in estimating the density. In integrating the occupation, the sources of uncertainty are the normalisation (discussed earlier), and the accuracy with which the critical pumping power has been determined. We may underestimate the experimental critical density if the nonlinear threshold we use is in fact associated with the diverging susceptibility on approaching the transition

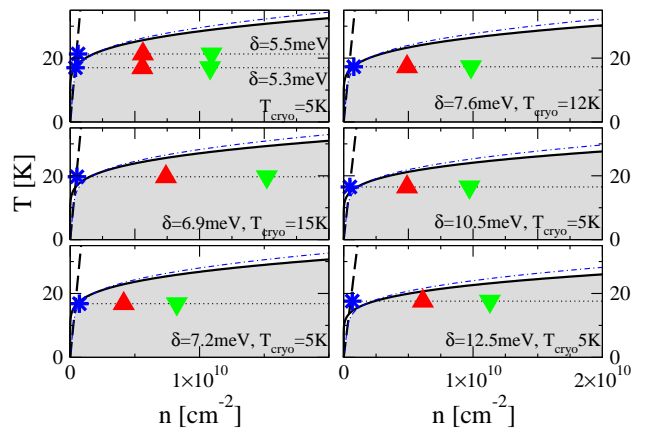


FIG. 3: (Color online) Theoretical phase diagram of temperature versus density (gray region is condensed) for different values of the detuning δ and T_{cryo} , with superimposed the estimates of density from the PL (blue stars) and from the blue-shift of LP (red upper and green lower triangles).

rather than with the condensation transition itself. As an upper bound on this source of uncertainty we note that the density when the linewidth reaches a minimum is between 1.6 and 2 times that at threshold. For the estimates from the blueshift, the uncertainties here are harder to quantify. The exclusion interaction for excitons may overestimate blueshift, implying our estimated density is too low. Alternatively, our calculation assumes a thermalised polariton distribution, whereas the influence of the exciton reservoir and hot carriers remains unclear within the present modelling, these might increase the blueshift, suggesting that our estimated density is too high. Finally, the theoretical phase boundary as yet neglects dephasing; it is this effect to which we next turn.

V. EFFECTS OF PUMP AND DECAY

As is apparent from Fig. 1, and the discussion in Ref.16, the polariton distribution is thermalised. However a thermalised population distribution does not necessarily imply that one can neglect effects^{19,38,39,40,41,42} of pumping and decay. To understand this distinction, let us consider two dimensionless ratios that characterise non-equilibrium effects. One might estimate the effect of pumping and decay by considering the ratio of polariton lifetime to thermalization time (e.g., ~ 2 in the current experiment, ~ 2000 in early atomic gas⁴³ BECs). When this ratio is larger than one, the distribution will be thermalised. However, even with a thermal polariton distribution, pumping and decay cause a particle flux, introducing dephasing, which increases the critical density at a given temperature.³⁸ The importance of this dephasing can be estimated by comparing the homogeneous photon linewidth, $\text{LW} \approx 1 \text{ meV}$, to the temperature $k_B T \approx 2 \text{ meV}$. As these parameters are comparable,

linewidths will have significant homogeneous contributions, and dephasing can affect the ability of the system to maintain a coherent state.

As an estimate of how such dephasing would modify critical density at a given temperature, Fig. 4 compares the phase boundaries found from calculations using model (1), but with photon decay and injection of excitons^{38,39} taken into account. These calculations introduce a flux of particles by allowing photons to decay and continually injecting new excitons to maintain a steady state. The departure from the closed system picture is controlled by two parameters, the photon decay rate $2\kappa = 1\text{meV}$, and a pumping rate γ that describes coupling between the polariton system and the reservoir of high energy excitons. The value of γ is not clearly known, but is bounded. For $\gamma \gg \kappa$ one has a polariton linewidth larger than the bare photon linewidth; for $\gamma \ll \kappa$ there is instability of the homogeneous condensate³⁹; a range of γ bounded by these consideration is shown for illustration in Fig. 4 — within these limits, the exact value of γ does not significantly shift the curves. Although these calculations use model (1), for tractability of the nonequilibrium calculations, a Gaussian distribution of excitonic energies ε_α and a constant coupling $g_{\alpha,\mathbf{k}} = \Omega_R/2$, are used. The main effect of this replacement is that there is no simple relation between the units of density for this calculation and those in the previous figures, hence the arbitrary units in Fig. 4. However, one may note that the form of the equilibrium boundary (black) in Fig. 4 is very similar to that in Fig. 3, and one may thus estimate the size of shift associated with pumping and decay. Dephasing shifts the phase boundary to higher densities; this would reduce the distance between the predicted phase boundary and the critical density estimated from the blueshift.

A. Condensate fraction

As a further illustration of how dephasing depletes the condensate, we compare experimental condensate fraction (Fig. 5) with the theoretical quasi-condensate fraction (evaluated at the mean-field level) with and without pumping and decay (Fig. 4). Although trapping negligibly affects the phase boundary (the properties of the phase boundary being dominated by interactions), trapping and finite size are important in allowing a non-zero condensate fraction.^{44,45} A quasi-condensate fraction can also be defined for an infinite two-dimensional system; its definition follows from the behaviour of the off-diagonal one-particle density matrix $\rho(r)$. In three dimensions $\rho(r)$ tends to a constant at long distances, which defines Off-Diagonal Long-Range order; in two dimensions it instead decays as a power law. However, the power law decay is due to phase fluctuations, and by separating the effects of phase fluctuations from the quasi-condensate depletion due to density fluctuations⁴⁶ one may extract a quasi-condensate density. In a trapped two-dimensional system there can be a regime near the phase transition

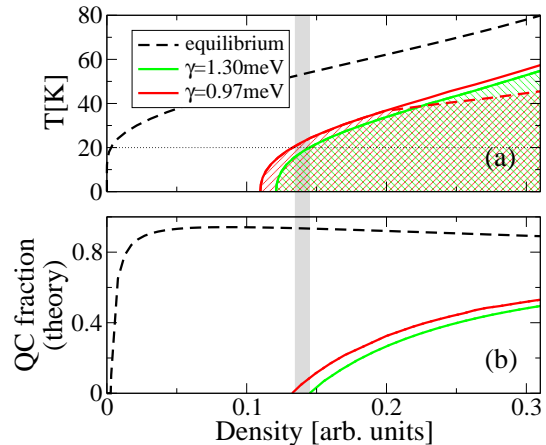


FIG. 4: (Color online) Critical temperature versus density (in arbitrary units) (panel a) and quasi-condensate fraction at $T = 20\text{K}$ (panel b) including the effects of pumping (rate γ) and decay, with decay rate for a homogeneous cavity linewidth of 1meV , for a model Gaussian distribution of the excitonic energies. In panel (a), for $\gamma = 0.97\text{meV}$ and high temperatures the nonequilibrium model has an instability of the homogeneous condensate³⁹; the boundary of this instability is marked by the dashed line, and the stable condensed region is marked by hatchings.

in which there is quasi-condensation; however as temperature is reduced or density increased, coherence will rapidly extend over the entire system.^{26,45} Thus, apart from a small region near the transition, coherence across the entire system is expected even when the phase transition itself is like the BKT transition.

The experimental condensate fraction is determined from the occupancies illustrated in the inset of Fig. 5 as follows: The occupancy shows a clear peak at low momentum; the experimental estimate of condensate fraction comes from the fraction of polaritons found in this low momentum peak, i.e. the integrated density within the FWHM of the occupancy peak, see Ref.47 for further details. The theoretical mean-field estimate is the ratio of the coherent density, $|\langle\psi\rangle|^2 + \sum_\alpha |\langle S_\alpha^- \rangle|^2$ to the total (mean-field) density of polaritons.³⁹ There are of course complications in comparing the experimental condensate fraction of a trapped 2D Bose gas⁴⁴ to the theoretical mean-field condensate fraction; however the comparison between the various mean-field estimates clearly shows that pumping and decay are responsible for a reduction of the quasi-condensate fraction.

VI. CONCLUSIONS

Concluding, we have compared experimental and theoretical phase boundaries for condensation of CdTe microcavity polaritons. The experimental data lie near the

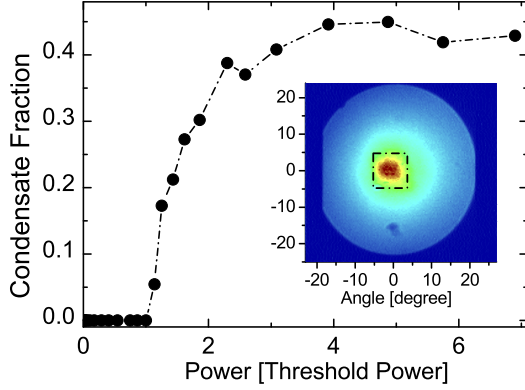


FIG. 5: (Color online) Experimental condensate fraction (the fraction of polaritons in the low momentum peak), at detuning $\delta = 10.5\text{meV}$, $T_{\text{cryo}} = 5.4\text{K}$, $T_{\text{eff}} = 16.5\text{K}$. Inset: Occupancy vs angle, showing the peak at small angles (low momentum), the integrated weight inside which is taken as condensate density.

crossover between a regime where the transition can adequately be described by condensation of structureless bosons and a mean-field regime where instead the long-range nature of the polariton-polariton interaction determines the boundary. We were limited to temperatures near this crossover region: Because of the short polariton lifetime, the polariton temperature is decoupled from that of the lattice. There are small differences between the various ways of estimating experimental density; were one to neglect effects of disorder these differences would have been an order of magnitude larger. However, these estimates of experimental density lie close to the theoretical phase boundary, and considering the effects of pump and decay improves this agreement.

Acknowledgments

JK, FMM and MHS would like to acknowledge the financial support of EPSRC, JMJK acknowledges financial support from Pembroke College, Cambridge.

APPENDIX A: INTERACTION BETWEEN SPINS AND BIEXCITONS

This appendix discusses the effect on the phase diagram of including an attractive interaction between opposite polarisations of two-level systems. The model used is a straightforward generalisation of Eq. (1), explicitly keeping track of the four possible configurations of each disorder-localised site; unoccupied, singly occupied by an exciton or occupied by a biexciton, thus each site has an

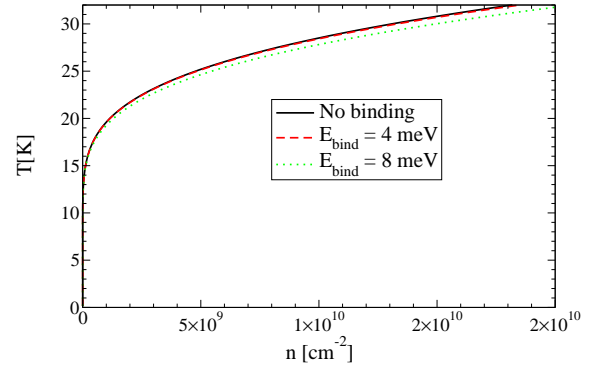


FIG. 6: (Color online) Mean-field phase boundary calculated with varying strengths of biexciton binding energy, with a detuning $\delta = 5.3\text{meV}$ (i.e. corresponding to top-left panel of Fig. 3).

effective Hamiltonian:

$$\hat{h}_\alpha = \begin{pmatrix} 0 & \Lambda_{\alpha,L} & \Lambda_{\alpha,R} & 0 \\ \Lambda_{\alpha,L}^* & \varepsilon_\alpha - \mu & 0 & \Lambda_{\alpha,L} \\ \Lambda_{\alpha,R}^* & 0 & \varepsilon_\alpha - \mu & \Lambda_{\alpha,R} \\ 0 & \Lambda_{\alpha,L}^* & \Lambda_{\alpha,R}^* & 2(\varepsilon_\alpha - \mu) - E_{XX} \end{pmatrix} \quad (\text{A1})$$

where $\Lambda_{(L,R),\alpha} = \sum_{\mathbf{k}} g_{\alpha,\mathbf{k}} \psi_{(L,R)\mathbf{k}} / \sqrt{A}$ describes the coupling of a given localised site to the left- or right-circularly polarised photon field, and E_{XX} is the biexciton binding energy. This expression replaces the combination $(\varepsilon_\alpha - \mu)S_\alpha^z + \sum_{\mathbf{k}} (g_{\alpha,\mathbf{k}} \psi_{\mathbf{k}} S_\alpha^+ + \text{h.c.}) / \sqrt{A}$ that appears in Eq. (1) for each site. The mean-field theory, analogous to Sec. III C is found by calculating the mean-field estimate of density which may be written as:

$$\rho = \frac{1}{A} \sum_{\alpha} \frac{2(z_\alpha + z_\alpha^2 \lambda)}{1 + 2z_\alpha + z_\alpha^2 \lambda}, \quad (\text{A2})$$

where we have defined:

$$\lambda = e^{\beta E_{XX}}, \quad z_\alpha = e^{-\beta(\varepsilon_\alpha - \mu)},$$

and the gap equation (found from the linear polarisability of the four-level system) becomes:

$$\omega_0 - \mu = \sum_{\alpha} \frac{|g_{\alpha,0}|^2 / A}{1 + 2z_\alpha + z_\alpha^2 \lambda} \left[\frac{1 - z_\alpha}{\varepsilon - \mu} + \frac{z_\alpha(1 - z_\alpha \lambda)}{\varepsilon - \mu - E_{XX}} \right]. \quad (\text{A3})$$

It is straightforward to see that if $E_{XX} = 0$, these two forms reproduce those in Eq. (3) and Eq. (4) respectively. A more complete treatment of binding ought to take account of how the binding strength varies according to the localised nature of the single exciton states, however to place a bound on how large a shift of critical temperature the biexciton binding might induce it is sufficient to consider this model with a constant biexciton binding.

Figure 6 shows the effect with binding energies up to 8meV, corresponding to the largest value seen for excitons bound at vicinal surfaces in CdTe/CdMgTe wells.⁴⁸

Such a value is almost certainly an overestimate for the samples used in current experiment, as the results of Ref.48 are for narrower quantum wells than the current experiment (3.2nm vs 5nm), and correspond to biexcitons with the greatest in-plane confinement. Even with this overestimate of biexciton binding, the effect of biexciton binding on the critical temperature can be seen to be small. Moreover, were biexcitons to play a sig-

nificant role, one would expect to see a crossover between the photoluminescence associated with exciton-polaritons and that from biexciton-polaritons, as was investigated in GaAs.⁴⁹ The fact that no such crossover is seen, and that the effects of biexciton binding on the mean-field phase boundary are small justify our neglect of biexciton physics in the rest of the paper.

-
- * Present address: School of Physics and Astronomy, Cardiff University, Queens Buildings, 5 The Parade, Cardiff, CF24 3AA, UK
- ¹ J. J. Hopfield, Phys. Rev. **112**, 1555 (1958).
 - ² C. Weisbuch, M. Nishioka, A. Ishikawa, and Y. Arakawa, Phys. Rev. Lett. **69**, 3314 (1992).
 - ³ A. Kavokin, G. Malpuech, and F. P. Laussy, Phys. Lett. A **306**, 187 (2003).
 - ⁴ G. Malpuech, et al., Semicond. Sci. Technol. **18**, S395 (2003).
 - ⁵ J. Keeling, Phys. Rev. B **74**, 155325 (2006).
 - ⁶ J. Keeling, P. R. Eastham, M. H. Szymańska, and P. B. Littlewood, Phys. Rev. Lett. **93**, 226403 (2004).
 - ⁷ F. M. Marchetti, J. Keeling, M. H. Szymańska, and P. B. Littlewood, Phys. Rev. Lett. **96**, 066405 (2006).
 - ⁸ D. Sarchi and V. Savona, Phys. Rev. B **77**, 045304 (2008).
 - ⁹ L. S. Dang, et al., Phys. Rev. Lett. **81**, 3920 (1998).
 - ¹⁰ H. Deng, et al., Science **298**, 199 (2002).
 - ¹¹ H. Deng, et al., P.N.A.S. **100**, 15318 (2003).
 - ¹² M. Richard, et al., J. Phys.: Condens. Matter **16**, S3683 (2004).
 - ¹³ M. Richard, et al., Phys. Rev. Lett. **94**, 187401 (2005).
 - ¹⁴ M. Richard, et al., Phys. Rev. B **72**, 201301 (2005).
 - ¹⁵ H. Deng, et al., Phys. Rev. Lett. **97**, 146402 (2006).
 - ¹⁶ J. Kasprzak, et al., Nature **443**, 409 (2006).
 - ¹⁷ J. Kasprzak, et al., Phys. Rev. B **75**, 045326 (2007).
 - ¹⁸ J. Kasprzak, et al., Phys. Rev. Lett. **100**, 067402 (2008).
 - ¹⁹ K. G. Lagoudakis, et al. (2008), arXiv:0801.1916.
 - ²⁰ H. Deng, et al., Phys. Rev. Lett. **99**, 126403 (2007).
 - ²¹ R. Balili, et al., Science **316**, 1007 (2007).
 - ²² S. Christopoulos, et al., Phys. Rev. Lett. **98**, 126405 (2007).
 - ²³ C. Ciuti, P. Schwendimann, and A. Quattropani, Semicond. Sci. Technol. **18**, S279 (2003).
 - ²⁴ F. M. Marchetti, J. Keeling, M. H. Szymańska, and P. B. Littlewood, Phys. Rev. B **76**, 115326 (2007).
 - ²⁵ J. Keeling, P. R. Eastham, M. H. Szymańska, and P. B. Littlewood, Phys. Rev. B **72**, 115320 (2005).
 - ²⁶ J. Keeling, F. M. Marchetti, M. H. Szymańska, and P. B. Littlewood, Semicond. Sci. Technol. **22**, R1 (2006).
 - ²⁷ E. Runge and R. Zimmermann, in *Advances in Solid State Physics*, edited by B. Kramer (Vieweg, Braunschweig, 1998), vol. 38, pp. 251–263.
 - ²⁸ P. R. Eastham and P. B. Littlewood, Solid State Commun. **116**, 357 (2000).
 - ²⁹ D. M. Whittaker, Phys. Rev. B **61**, R2433 (2000).
 - ³⁰ A. Baas, et al. (2007), arXiv:0712.2121.
 - ³¹ D. R. Yakovlev, et al., Phys. Rev. Lett. **79**, 3974 (1997).
 - ³² A. Griffin, D. Snoke, and S. Stringari, eds., *Bose-Einstein Condensation* (Cambridge University Press, Cambridge, 1995).
 - ³³ J. M. Kosterlitz and D. J. Thouless, J. Phys. C: Solid State Phys. **6**, 1181 (1973).
 - ³⁴ D. R. Nelson and J. M. Kosterlitz, Phys. Rev. Lett. **39**, 1201 (1977).
 - ³⁵ W. Ketterle and N. J. van Druten, Phys. Rev. Lett. **54**, 656 (1996).
 - ³⁶ V. Bagnato and D. Kleppner, Phys. Rev. A **44**, 7439 (1991).
 - ³⁷ M. Holzmann, G. Baym, J.-P. Blaizot, and F. Lalœ, P.N.A.S. **104**, 1476 (2007).
 - ³⁸ M. H. Szymańska, J. Keeling, and P. B. Littlewood, Phys. Rev. Lett. **96**, 230602 (2006).
 - ³⁹ M. H. Szymańska, J. Keeling, and P. B. Littlewood, Phys. Rev. B **75** (2007).
 - ⁴⁰ M. Wouters and I. Carusotto, Phys. Rev. A **76**, 043807 (2007).
 - ⁴¹ M. Wouters, I. Carusotto, and C. Ciuti, Phys. Rev. B **77**, 115340 (2008), arXiv:0707.1016.
 - ⁴² J. Keeling and N. G. Berloff (2007), arXiv:0706.3686.
 - ⁴³ K. B. Davis, et al., Phys. Rev. Lett. **75**, 3969 (1995).
 - ⁴⁴ M. Bayindir and B. Tanatar, Phys. Rev. A **58**, 3134 (1998).
 - ⁴⁵ D. S. Petrov, M. Holzmann, and G. V. Shlyapnikov, Phys. Rev. Lett. **84**, 2551 (2000).
 - ⁴⁶ Y. Kagan, et al., Phys. Rev. A **61**, 043608 (2000).
 - ⁴⁷ J. Kasprzak, Ph.D. thesis, Universite Joseph Fourier, Grenoble (2006).
 - ⁴⁸ L. Besombes, K. Kheng, and D. Martrou, Phys. Rev. Lett. **85**, 425 (2000).
 - ⁴⁹ M. Saba, et al., Phys. Rev. Lett. **85**, 385 (2000).